Fade Slope Analysis of Ka-Band Earth-LEO Satellite Links Using a Synthetic Rain Field Model

Weiwen Liu and David G. Michelson, *Senior Member, IEEE*

***Abstract*—Because the motion of a low Earth orbit (LEO) satellite across the sky causes the Earth-space path to very quickly pass through any rain cells in the vicinity, the degree of rain fading on such paths changes more rapidly and leads to steeper fade slopes than in the geostationary case. Because comprehensive measurement data have not yet been compiled for fading on LEO links in the Ka-band, we have used simulations based on Goldhirsh's method for determining the key parameters of the well-known EXCELL model of a horizontal rain structure from long-term global rain statistics to obtain plausible estimates of the fade slope distributions for selected scenarios. The results that we obtained for geostationary satellites closely match those observed at selected sites during the Advanced Communications Technology Satellite program. The results that we obtained for LEO satellites show how fade slopes will steepen as 1) the altitude of the satellite decreases; 2) the frequency band of operation increases; and 3) the average rain rate increases. Furthermore, they suggest that, at a given probability level, the fade slopes could be between two and ten times greater than those for geostationary satellites and that mobile terminals with a clear view of the sky will experience fade slopes that are similar to those encountered by fixed or transportable terminals. These results have important implications for the design of power control algorithms and other fade-mitigation techniques.**

***Index Terms*—Fading channel, Ka-band, millimeter-wave radio propagation meteorological factors, satellite communications.**

I. Introduction

ALTHOUGH rain fading on Earth-space links is particularly troublesome in the Ka-band, moving to higher frequencies offers many potential advantages, including a less-congested spectrum, the possibility of supporting higher system bandwidths (and higher data rates), reduced interference potential, and smaller equipment size (particularly smaller antennas) compared with lower frequencies [1]. At present, most Ka-band Earth-space links are used to increase the capacity of conventional communications satellites located in geostationary Earth orbit (GEO). In recent years, however, system designers have begun to show serious interest in using Ka-band links to provide high-speed data communications with satellites in low Earth orbit (LEO) during the relatively short time that a LEO satellite passes within the range of an Earth station.

Manuscript received February 29, 2008; revised July 6, 2008. This work was supported in part by MacDonald Dettwiler and Associates, by Western Economic Diversification Canada, and by the Natural Sciences and Engineering Research Council of Canada. The review of this paper was coordinated by Dr. D. Zhao.

The authors are with the Department of Electrical and Computer Engineering, University of British Columbia, Vancouver, BC V6T 1Z4, Canada (e-mail: weiwenl@ece.ubc.ca; davem@ece.ubc.ca).

Digital Object Identifier 10.1109/TVT.2008.2004766

In the late 1990s, Iridium Satellite LLC pioneered the use of Ka-band Earth-space links to LEO with the establishment of several Ka-band terrestrial gateways to their constellation of 66 LEO communications satellites. (Following a major operational restructuring, only two gateways remain in operation.) Taiwan's ROCSAT-1 [2] and Australia's FedSat [3], [4] have both recently carried experimental Ka-band transponders into LEO, although only results from the latter have been reported in the literature to date. In the near future, MacDonald Dettwiler's Cascade system will use high-speed Ka-band Earth-space links to support a LEO-based store-and-forward data delivery system that will allow end users to transfer terabytes of data between any two locations on Earth within 24 h [5], [6]. Meanwhile, the European Space Agency is taking the first steps to relieve the congested high-rate downlink band at 8.2 GHz (X-band) that is currently used by LEO-based Earth observation satellites by opening an alternative high-rate downlink band at 26 GHz (Ka-band) [7].

Because the rapid motion of a LEO satellite across the sky causes the Earth-space path to very quickly pass through rain cells in the vicinity, the degree of rain fading on LEO satellite links changes more rapidly and, as we shall show, leads to steeper fade slopes than in the well-studied case of links to geostationary satellites, e.g., [8]–[12]. This has important implications for the performance of the power control algorithms, forward error correction schemes, and other techniques used to mitigate such fading. However, any plans that the National Aeronautics and Space Administration or European Space Agency might have had, following the completion of the successful geostationary Ka-band measurement programs in the 1990s, to conduct programs aimed at characterizing fading on Ka-band LEO links, were never realized. Although Iridium LLC may have collected propagation data at a handful of the Ka-band gateways that they have operated since the late 1990s, none has been published or referred to in the open literature [13]. Sample data from several FedSat passes over Australia were reported in 2005 [3], [4], but little else has been released to date. The resulting dearth of information concerning the rate of fading experienced on Ka-band links to LEO satellites places system designers at a severe disadvantage.

Until more extensive measurement programs are undertaken, simulation based on reasonable models of the horizontal and vertical structures of rain is the likely best option for assessing the severity of fade slope due to rain fading on Ka-band links to LEO satellites. Several methods for generating realistic synthetic rain fields that are suitable for use in simulations of satellite communications systems have been proposed in recent years, e.g., [14]–[19]. In the past, such rain field models have

generally been used to predict outage probability at a given location or to assess the performance of site diversity between terminals with wide geographic separation. To the best of our knowledge, we are among the first to use such models for fade slope prediction.

Here, we seek to obtain plausible estimates of the manner in which the fade slope distribution experienced on Ka-band links from a fixed station to a satellite in LEO is likely to be affected by the following: 1) the altitude of the satellite; 2) the carrier frequency; and 3) the long-term rain statistics in the vicinity of the Earth station. For simplicity, we use Goldhirsh's method [15] to obtain the key parameters of the well-known EXCELL model [14] of horizontal rain structure from long-term global rain statistics, together with details concerning the rain layer that have been captured by the relevant International Telecommunications Union Radiocommunication Sector (ITU-R) recommendations. We have accounted for advection of the rain cells by the wind by introducing a wind velocity model based on the assumptions that the average wind speed is lognormally distributed and that the average wind direction is uniformly distributed. Because we base our simulations on global rain statistics, our approach may be used to assess the performance of links between LEO satellites and Earth stations located at essentially any location and in any climatic region on Earth.

The remainder of this paper is organized as follows: In Section II, we briefly describe the elements of our simulation scenario, including issues peculiar to studies of Earth-LEO satellite links and aspects of rain field modeling that should be considered when estimating fade slope. In Section III, we describe our simulation procedure including our simplifying assumptions. In Section IV, we present our results. Finally, in Section V, we summarize our findings and draw conclusions.

II. Formulation of the Simulation Scenario

A. Satellites in LEO

When formulating the link budget and predicting the reliability of a fixed link to a satellite in GEO, it is sufficient to specify the local rain statistics and the elevation angle of the satellite, as seen by the Earth station.[1] When considering a link to a satellite in a LEO, however, the situation is more complicated. The orbital altitude may range from 200 to 2000 km, and the inclination angle may range from 0° (equatorial) to 90° (polar) to slightly beyond (sun-synchronous). The orbital altitude affects the minimum and maximum ranges to the satellite during each pass and the rate at which the satellite moves across the sky, as seen by the Earth station. The inclination angle, combined with the latitude of the Earth station, affects the probability distribution function of the satellite's elevation angle, as seen by the Earth station [20]. Thus, before proceeding, we need to limit the number of cases that we consider by identifying LEOs of particular relevance or significance.

A histogram of the orbital altitudes of a representative set of 369 communications, Earth observation, and research satellites currently in LEO, based on two-line element (TLE) data sets obtained from Celestrack [21], is given in Fig. 1. The lowest practical orbit has an altitude of 200 km; below that, atmospheric drag severely limits orbital lifetime. The majority of LEO satellites occupy orbits having altitudes near 800 and 1500 km, with communications satellites having the smallest spread in orbital altitude and research satellites having the greatest. Further examination of the TLE data sets also reveals that the vast majority of the LEO-based Earth observation and research satellites, and perhaps half of the LEO-based communications satellites, are in near-polar circular orbits (including sun-synchronous orbits). In light of this, and for the sake of simplicity, we have focused our initial fade slope characterization efforts on LEO satellites in circular polar orbits with altitudes of 200, 800, and 1500 km. However, our approach can easily be applied to LEO satellites at other altitudes and inclinations, including those in elliptical orbits.

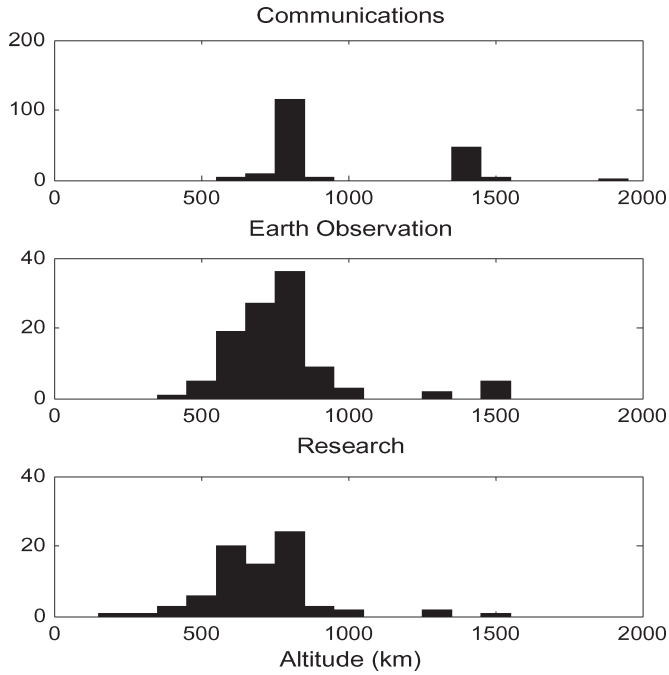

Fig. 1. Distribution of the altitudes of 369 communications, Earth observation, and research satellites in LEO.

B. Fast and Slow Variations in Path Loss on Ka-Band Earth-Space Links

Over time, various processes will cause the received signal strength on Ka-band Earth-space links to vary over both fast and slow time scales. Fast fading is usually associated with processes such as scintillation due to turbulence in the atmosphere and multipath scattering from nearby obstacles and scatterers (buildings, trees, and foliage) in relative motion with respect to the Earth station. Slow fading, which is our primary interest in this paper, is associated with the following:

1) evolution of the individual rain cells that comprise the rain field, including changes in the physical extent of the cell(s), rain rate, and drop size distribution;
2) motion of the rain cells with respect to the Earth station due to advection by wind;

[1]The elevation angle of a GEO satellite, as seen by the Earth station, determines the range to the satellite.

TABLE I
PROCESSES THAT CAUSE SLOW VARIATION OF SIGNAL STRENGTH ON EARTH-SPACE LINKS

	Rain event evolution	Storm motion	Terminal motion	Range variation	Az-el variation
Fixed to GEO	X	X			
Mobile to GEO	X	X	X		
Fixed to LEO	X	X		X	X
Mobile to LEO	X	X	X	X	X

3) movement of the ground terminal with respect to Earth;
4) rapid changes in the range to the satellite (and the length of the slant path through the atmosphere and the rain layer) as the satellite passes across the sky;
5) rapid changes in the azimuth and elevation angle of the Earth-space path (and the intersection of the path with individual rain cells) as the satellite passes across the sky.

The significance of the five slow-fading processes for different user scenarios is summarized in Table I.

1) For the well-studied case of fixed links to satellites in geostationary orbit, only rain cell evolution and storm motion are significant. Synthetic storm techniques are an effort to distinguish between these two processes, based on measurements of the received signal strength data or point rain rate and estimates of local wind speed and direction [22], [23].
2) The case of links from mobile terminals to satellites in geostationary orbit has been considered by others in recent years, e.g., in [23] and [24]. In such cases, the movement of the terminal with respect to both the storm and nearby structures that may temporarily block the path must also be accounted for.
3) In the case of fixed links to LEO, changes in the length of the slant path and rapid changes in the total amount of rain observed along the path as the satellite passes across the sky must be accounted for.
4) In the case of mobile links to LEO, all five of the processes previously identified must be accounted for.

C. Fade Slope Analysis and Rain Field Modeling

Fade slope analysis is traditionally conducted using measured received signal strength data, whereas synthetic rain fields, which depict the simulated 2-D distribution of rain rate over a certain area, are normally used in conjunction with wind velocity models to evaluate outage probabilities on single links and mutual correlation between outages at geographically separated sites, i.e., site diversity. This work is apparently among the first to use synthetic rain field models to predict fade slope distributions.

Synthetic rain fields model the spatial structure of rain on three scales: 1) small scale ($\sim 20 \times 20$ km^2)—the shape and intensity profiles of individual rain cells; 2) medium scale ($\sim 150 \times 150$ km^2)—the random distribution of individual rain cells over small areas; and 3) large scale ($\sim 1000 \times 1000$ km^2)—the distribution of rain cell clusters due to the formation of weather fronts [18]. Because fade slope is determined by differences in rain intensity at points within the field that are typically less than 100 m apart, the spatial distribution of the rain cells is unlikely to play a significant role in determining the fade slope distribution. However, it seems likely that the fade slope distribution will be affected, to at least some degree, by the profile of the individual rain cells.

A rain cell is commonly defined as the region surrounding a local maximum within which the rain rate is larger than a certain threshold [16]. In recent years, three alternative rain cell models have been developed based on radar observations of rain cells, which show that the rain rate in the outer regions of individual rain cells tends to exponentially decay. The EXCELL model, which is the simplest of the three models, assumes that the rain cell has an exponential profile with a prominent central peak [14], i.e., the rain rate distribution in the horizontal plane is given by

$$R(r) = R_M \exp\left(-\frac{r}{\rho_0}\right) \text{ (in millimeters per hour)} \quad (1)$$

where R_M is the peak rain rate, r is the horizontal distance from the center of the cell, and ρ_0 is the distance scale factor. The Lowered EXCELL model is a recent variant of the EXCELL model that applies to stratiform rain [19]. The rain rate distribution in the horizontal plane is given by

$$R(r) = \left\{ \begin{array}{ll} (R_M + R_{\text{low}} \exp\left(-\frac{r}{\rho_0}\right) - R_{\text{low}}, & r \le r_{\max} \\ 0, & r > r_{\max} \end{array} \right\}$$

(in millimeters per hour) (2)

where R_M is the peak rain rate, R_{low} is the so-called lowering factor, r is the horizontal distance from the center of the cell, and ρ_0 is the distance scale factor. The HYCELL model, which is the most complicated of the three, models the rain rate distribution in the horizontal plane as

$$R(x,y) = \left\{ \begin{array}{ll} R_G \exp\left(-\left(\frac{x^2}{a_G^2} + \frac{y^2}{b_G^2}\right)\right), & r \le r_1 \\ R_E \exp\left(-\left(\frac{x^2}{a_E^2} + \frac{y^2}{b_E^2}\right)^{1/2}\right), & r_2 \le r < r_1 \end{array} \right\}$$

(in millimeters per hour) (3)

where R_G, a_G, and b_G define the Gaussian component, and R_E, a_E, and b_E define the exponential component [16]. This substantially reduces the amplitude of the central peak. Coordinates x and y and radial distance r are measured with respect to the center of the cell.

Our ultimate goal is to assess the sensitivity of the fade slope statistics to the degree of detail captured by these models. Here, we have started simply by using an approach based on the EXCELL and ITU-R one-layer rain models. As we shall note later, the next logical step will be to complete the assessment by conducting simulations using the more complicated rain cell models and rain layer models, e.g., [22] and [25].

III. Simulation Model

A. Approach and Simplifying Assumptions

We used Goldhirsh's method [15] to generate synthetic rain fields based on long-term global rain statistics. The *absolute probability* of rain falling at a given rate is self-explanatory. The *conditional probability* refers to the probability of rain falling at a given rate over all instances when the rain rate exceeds a given threshold, e.g., 0.5 mm/h.

The major steps of Goldhirsh's method for generating a 2-D rain field are given here.

1) For a specific location, determine the absolute complementary cumulative distribution function (CCDF) of rain rate, as specified by Rec ITU-R P. 837.
2) Set a rain rate threshold.
3) Determine the conditional CCDF by dividing the absolute CCDF by the absolute probability of the rain rate equaling the specified threshold. (The typical absolute and conditional CCDFs for Tampa and White Sands are shown in Fig. 2.)
4) Estimate the parameters P_0, R^*, and κ by fitting the resulting conditional CCDF to

$$P(R_q) = P_0 \left[\ln \left(\frac{R^*}{R_q} \right) \right]^{\kappa} \tag{4}$$

where R_q is an arbitrary threshold level of rain rate, $P(R_q)$ is the probability that the rain rate is greater than R_q, and where R^* is several times greater than the maximum measured rain rate.

5) Determine the peak rain rate values R_M by setting the minimum peak rain rate, i.e., 2.5 mm/h, and the peak rain rate interval, i.e., 5 mm/h.
6) Calculate the number of rain cells belonging to a certain peak rain rate interval, using

$$N(R_M) = \left(\frac{P_0}{2\pi\rho_0^2 R_M} \right) \kappa(\kappa-1)(\kappa-2) \left[\ln \left(\frac{R^*}{R_M} \right) \right]^{\kappa-3} \tag{5}$$

$$\rho_0(R_M) = \frac{10 - 1.5 \log 10 R_M}{\ln \left(\frac{R_M}{R \min} \right)} \tag{6}$$

$$NUM(R_Q) \approx \left(\frac{N(R_M) + N(R_M + \delta)}{2} \right) \delta A_0 \tag{7}$$

where ρ_0 is the "characteristic distance" from the rain cell center to the bound that the rain rate reduces to $\exp(-1)$ of the peak value, $N(R_M)$ is the rain cell number density for a certain peak rain rate, δ is the peak rain rate interval, A_0 is the observation area, Q is the index denoting the cells with peak rain rate within the interval, and $NUM(R_Q)$ is the number of rain cells with a certain peak rain rate ranging from R_M to $R_M + \delta$.

7) Randomly distribute the rain cells $(\text{CELL}_1, \text{CELL}_2, \ldots, \text{CELL}_{NUM(R_Q)})$ throughout the rain field A_0.
8) Specify the grid points within A_0 every 0.5 km $\times$ 0.5 km, starting with the grid location (0.25 km, 0.25 km), and for each grid point, calculate the rain rates contributed from all $NUM(R_Q)$ rain cells based on the EXCELL model and sum them to yield the rain rate due to rain cells within the specified peak rain rate interval

$$R_Q(x, y) = \sum_{N=1}^{N_{\max}} R_{Q,N}(x, y) \tag{8}$$

where (x, y) is the location of the grid point, and $N_{\max}$ is equal to $NUM(R_Q)$.

9) Repeat procedures 7) and 8) for $Q = 2, 3, \ldots, Q_{\max}$. The total rain rate at each grid point is given by

$$R(x, y) = \sum_{Q=1}^{Q_{\max}} R_Q(x, y). \tag{9}$$

We are then able to generate the rain rate values for all points in the grid in the form of a matrix that gives the rain rate throughout the rain field A_0.

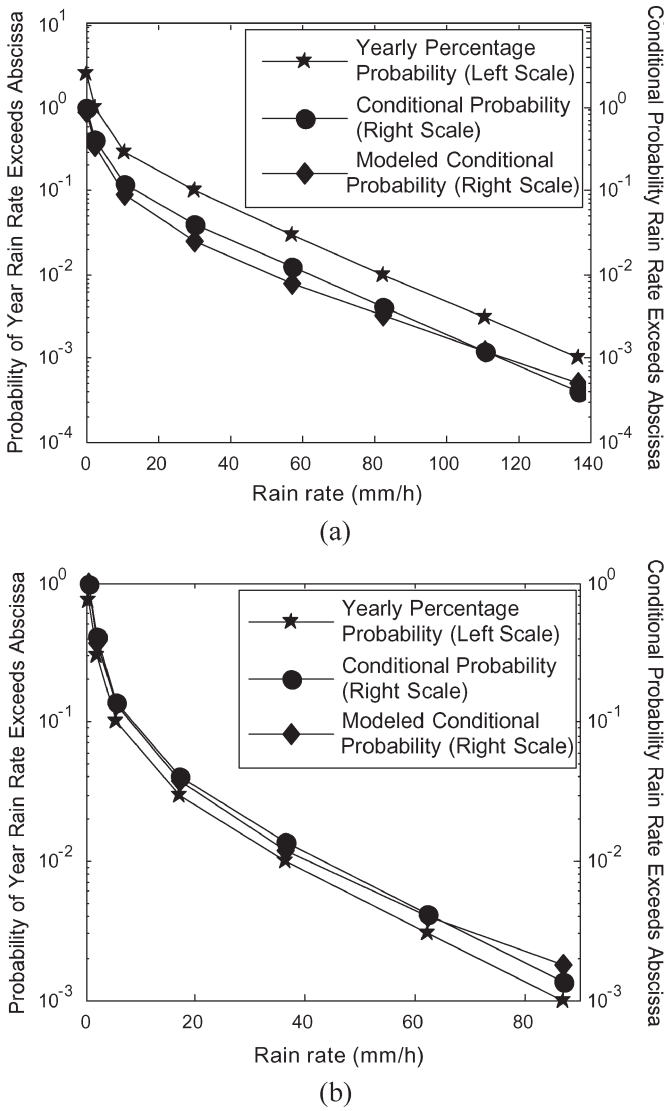

Fig. 2. (Curve with stars) Percentage of the year that the rain rate exceeds the abscissa, (curve with circles) probability of exceeding the abscissa, given that the rain rate exceeds 0.5 mm/h, and (curve with diamond) modeled conditional distribution. (a) Tampa, FL. (b) White Sands, NM.

TABLE II
RAIN FALL INTENSITY STATISTICS AT SELECTED LOCATIONS

Percentage of Time (%)	Rainfall intensity exceeded (mm/h)			
	White Sands, NM		Tampa, FL	
	Rain Zone E	P.837-5	Rain Zone N	P.837-5
1	0.6	0.2	5	2.4
0.3	2.4	1.9	15	11.1
0.1	6	5.7	35	30.6
0.03	12	17.0	65	57.2
0.01	22	36.4	95	82.6
0.003	41	62.2	140	110.9
0.001	70	87.3	180	136.9

Although Goldhirsh used the rain statistics from Rec ITU-R P. 837-1 that divides the globe into 15 rain zones, ITU-R has since replaced this by global rain statistics obtained from the European Centre for Medium-Range Weather Forecast (ECMWF) ERA-40 reanalysis database, as described in Rec ITU-R P.837-5. The rain rate intensity distributions for Tampa, FL (27.97° N, 82.53° W, in former ITU-R rain zone N), and White Sands, NM (32.38° N, 106.48° W, in former ITU-R rain zone E), which were obtained using the two approaches, are compared in Table II. The difference is small but noticeable. We generated absolute CCDFs based on Rec ITU-R P.837-5, instead of the earlier version, and follow the remaining steps in Goldhirsh's method to generate the 2-D rain field.

In the absence of detailed information concerning temperature or drop size distribution, we use the method specified in Rec ITU-R P. P.838 with which the specific attenuation γ_R (in decibels per kilometer) is obtained using the power-law relationship, i.e.,

$$\gamma_R = kR^\alpha \tag{10}$$

where R is the rain rate (in millimeters per hour), and k and α are coefficients that depend on frequency. We specify other details of the rain layer, such as its vertical extent, based on the relevant ITU-R recommendations, e.g., Rec ITU-R P.839. We account for advection of the rain cells due to wind by introducing a wind velocity model based on the commonly held assumptions of lognormally distributed wind speed [22] and uniformly distributed wind direction. We define a pass as that portion of the orbit that carries the satellite to 10° or greater above the horizon, as seen by the Earth station. Given that the rain layer is usually a few thousand meters in height [26], [27], we can use a flat Earth model without incurring significant errors in our estimate of the length of the slant path at low elevation angles.

Because the satellites are in LEO, the duration of individual passes, when the elevation angle is greater than 10° above the horizon, is on the order of minutes or tens of minutes. We generated pass durations for satellites in 200-, 800-, and 1500-km polar orbits for an Earth station located at latitude 30°, using a commercial satellite orbit prediction tool called AGI's Satellite Tool Kit (STK). The CCDFs of the pass duration are shown in Fig. 3. A more detailed summary of the pass statistics that includes the Earth stations at the 0°, 45°, and 60° latitudes is presented in Table III. Because pass durations are generally only minutes in length, we can reasonably assume that neither of the average wind speed and direction, the individual rain cells, and the average rain rates appreciably changes or evolves during each pass.

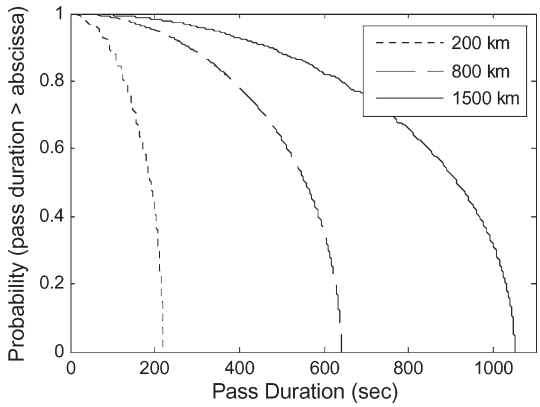

Fig. 3. CCDFs of the pass durations for LEO satellites in 200-, 800-, and 1500-km polar orbits, as seen by an Earth station at latitude 30°.

B. Simulation Procedure

We begin our simulation by specifying the Earth station's latitude and longitude and then determining the rain rate CCDF from the ECMWF ERA-40 reanalysis database, as specified in Rec ITU-R P.837. We then use Goldhirsh's method with the modifications described in the previous section to generate the 2-D rain field. As suggested by Goldhirsh, we truncate the horizontal extent of the exponential rain cell profile by setting a minimum rain rate. A representative rain field based on the parameters for Tampa, FL (27.97° N, 82.53° W), is shown in Fig. 4(a). The corresponding rain rate statistics for this location is given in Table II. Finally, we estimate the height of the rain field using the procedure outlined in Rec ITU-R P.839 so that we can convert the 2-D rain field into a 3-D rain field. The path length through the rain layer is a function of both the rain height and the elevation angle. As a result, the total rain attenuation along the path is given by

$$A = \gamma_{\text{eff}} \cdot \frac{h}{\sin\theta} \tag{11}$$

where h is the rain height, θ is the elevation angle, and γ_{eff} is the mean value of specific attenuation along the path.

We assume that the Earth station is fixed at a particular latitude and longitude and has a clear view of the satellite during the entire portion of the pass that is at least 10° above the horizon. We place the Earth station at the center of the rain field and then select the altitude and inclination of the satellite orbit. We use STK to generate range, elevation, and azimuth angle predictions at 1-s intervals for many successive passes.

At the beginning of each pass, we randomly generate the speed and direction of the wind during the pass. Past work has suggested that, over the long term, the average wind speed in the midtroposphere in Europe and North America is well modeled by the lognormal distribution with a median value of 30 km/h (8.33 m/s) and a standard deviation of $\log_e 2$ [22]. We use these

TABLE III
TYPICAL PASS STATISTICS FOR A SATELLITE IN LOW POLAR ORBIT

Satellite altitude (km):	200 km			800km			1500 km		
Earth station latitude (deg):	0	45	60	0	45	60	0	45	60
Average no. of passes per month.	40	59	85	91	133	197	114	168	277
Cumulative duration per month (min)	112	173	255	764	1116	1648	1575	2322	3644
Average duration per pass (min.)	2.8	2.9	3	8.4	8.4	8.4	13.8	13.8	13.2
Average velocity across the top of the rain layer (km/h)	1215	1173	1134	405	405	405	246	246	258

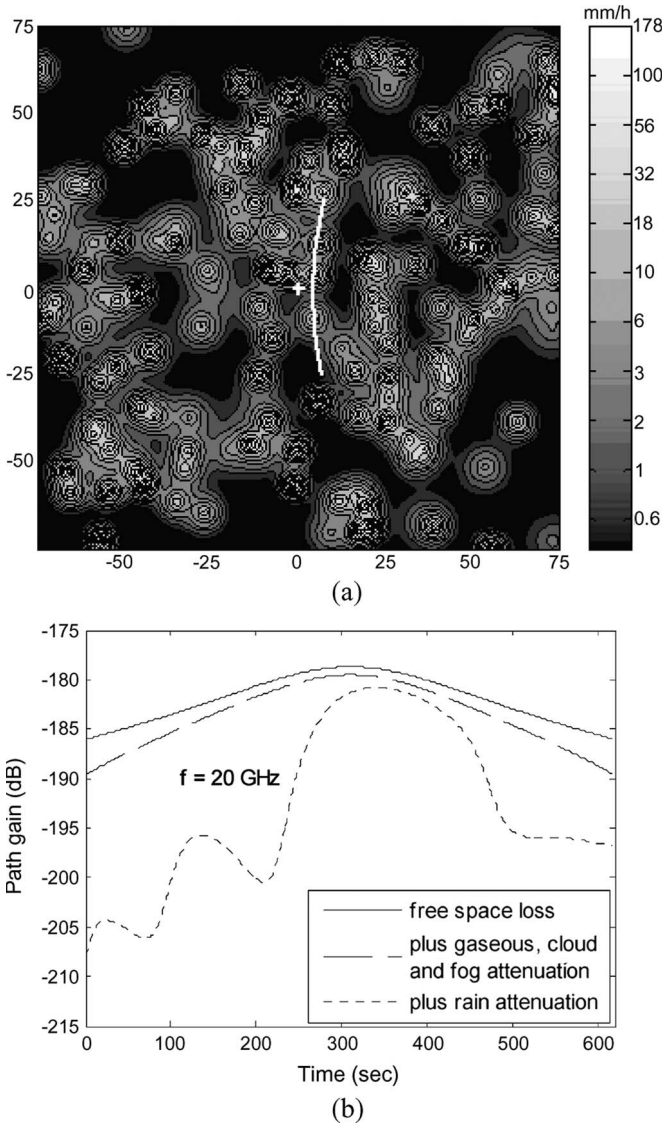

Fig. 4. Simulated pass of a LEO satellite at an altitude of 800 km over Tampa, FL, in the former ITU-R rain zone N. (a) Simulated 150 km × 150 km rain-rate field: (+) Earth station location and (-) the intersection of the path with the top of the rain layer. (b) Path gain observed at 20 GHz during the pass.

values here but set a realistic upper limit on the wind speed of 100 km/h. During the several minutes of each pass, we simulate advection of the rain field by the wind by sliding the rain field past the Earth station at a constant rate in the specified direction.

At any given instant, the total path loss L_p in decibels on Earth-space links is given by the sum of several terms including attenuation due to the following: 1) propagation through free space L_f; 2) atmospheric gases L_g; 3) cloud and fog L_c; and 4) rain L_r, i.e.,

$$L_p = L_f + L_g + L_c + L_r. \tag{12}$$

As the satellite sweeps across the sky, we determine the free-space path loss using the Friis transmission formula and estimate attenuation due to atmospheric gases, cloud, and fog using the methods outlined in Rec ITU-R P.676, P.836, and P.840, respectively. We then determine the intersection of the Earth-space path with rain cells in the vicinity. We divide the slant path through the rain layer into short segments and determine the average rain rate R_i for each of them. We predict the specific attenuation due to rain at each segment of the path using the method outlined in Rec ITU-R P. 838 and then sum the contributions of each segment to yield the total rain attenuation in decibels, as expressed by

$$L_r = \sum_i \gamma_{R_i} \Delta l \tag{13}$$

where γ_{R_i} is the specific attenuation corresponding to rain rate R_i, and Δl is the length of segment of the path. The simulation model geometry is shown in Fig. 5. In this manner, we determine the total path loss experienced along the path at successive instants during the satellite pass. Analysis of the time series over successive passes allows us to characterize slow fading due to rain, and the resulting fade slope, on Ka-band LEO satellite links.

C. Typical Results

A typical plot of path gain versus time for a link between an Earth station located near Tampa, FL (27.97° N, 82.53° W), and a satellite in an 800-km polar orbit is shown in Fig. 4(b). It corresponds to the scenario shown in Fig. 4(a). During this pass, the elevation angle ranged from 10° to 48°, and the distance between the satellite and the Earth station ranged from 1020 to 2400 km. We present the results in terms of path gain rather than path loss so that the curves will have the same form as those corresponding to the received power. The simulated pass resembles, at least superficially, observations of the received

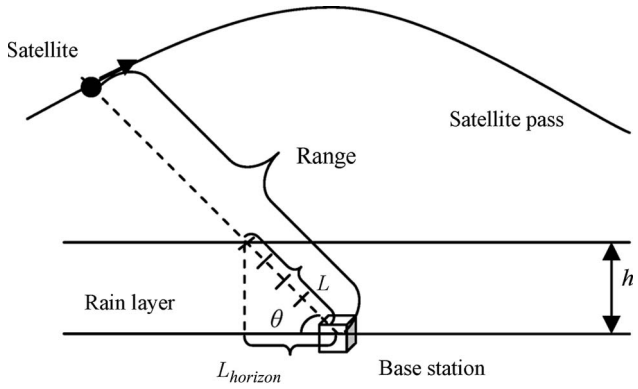

Fig. 5. Simulation model geometry. h is the rain height, L is the slant path length through the rain layer and is divided into small segments, L_{horizon} is the length of the horizontal projection of slant path, and θ is the elevation angle.

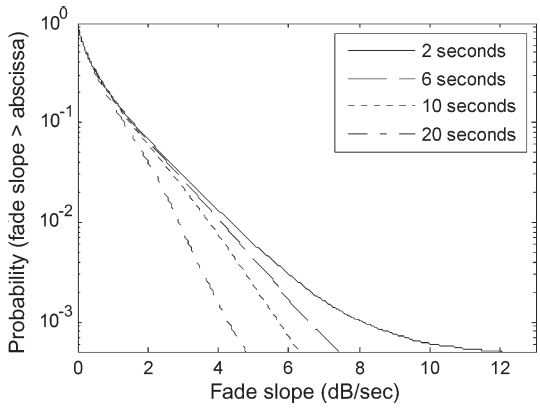

Fig. 6. Effect of fade slope interval on the estimation of steep fade slopes.

signal strength made during FedSat passes over Australia, as reported in [3] and [4].

IV. Result

A. Simulation Database

We used the path loss simulator described in the previous section to generate a time series of path loss applicable to satellites in polar orbits at altitudes of 200, 800, and 1500 km, as seen by fixed Earth stations at locations that correspond to White Sands, NM (32.38° N, 106.48° W), and Tampa, FL (27.97° N, 82.53° W). We ran each simulation until the cumulative duration of the passes over each site exceeded 420 h or 1.5 million s. For the 200-, 800-, and 1500-km orbits, this required almost 9000, 3000, and 1900 passes, respectively. From Table III, it would take approximately 12 years, 2 years, and 1 year, respectively, to achieve a similar cumulative duration of measurement data over a particular site using a single satellite.

B. Data Reduction Strategy

Rec ITU-R P.1623 offers recommendations for characterizing fade dynamics on Earth-space paths, including the characterization of fade slope or the rate of change of attenuation with time. A negative fade slope implies a rising signal, whereas a positive fade slope implies a falling signal. Other parameters of interest include fade duration, i.e., the time interval between two crossings above the same attenuation threshold, and interfade duration, i.e., the time interval between two crossings below the same attenuation threshold.

For Earth-space links to GEO, the range to the satellite and the length of the slant path through the atmosphere is fixed, and the satellite is visible continuously, making long observation times extremely practical. However, Earth-space links to LEO introduce two complications: First, the range to the satellite and the length of the slant path through the atmosphere is constantly changing during a pass. This makes it necessary to distinguish between attenuation with respect to free space and attenuation with respect to clear air (ACA) when defining fade slope on such links. Second, the satellite pass will last for several minutes at most, as shown in Fig. 3. The passes are generally so short compared with the duration of typical fading events that it is difficult to extract meaningful estimates of the fade and interfade durations because of the possibility that the rain attenuation only decreases or increases during a pass. Accordingly, our focus here is on the estimation of fade slope statistics based on sample intervals of 2 s. Not only is knowledge of fade slope useful to those engaged in the analysis and design of fade mitigation techniques, but it is also easily estimated, regardless of the longer term variations in the fade depth. The fade slope is defined by

$$\varsigma(t) = \frac{A\left(t + \frac{1}{2}\Delta t\right) - A\left(t - \frac{1}{2}\Delta t\right)}{\Delta t} \tag{14}$$

where $A(t)$ is the attenuation level in decibels at a given instant, and Δt is the time interval over which fade slope is calculated. We present our results in the form of CCDFs of the fade slope distributions. Those presented here are conditional, i.e., the vertical axis is the probability that the abscissa is exceeded, given that it is raining.

When working with measured data, high-frequency scintillation must be filtered from the received signal before one can estimate fade slope. Given the bandwidth of the scintillation process, one cannot choose an arbitrarily small value of Δt; ITU-R recommends a minimum value of 2 s. In Fig. 6, we present the CCDFs for a simulated Earth-space link where the Earth station is at a location that experiences higher than average rainfall. The link is occasionally experiencing fade slopes of several decibels per second (which is many times higher than one would likely observe on a link to GEO), where fade slope has been calculated using time intervals of 2, 6, 10, and 20 s. It is apparent that the use of time intervals greater than 2 s in length impairs our ability to resolve the steeper fade slopes that are characteristic of links to LEO, unless appropriate postprocessing, as specified in Rec ITU-R P.1623, is applied. Those conducting measurement campaigns aimed at characterizing fade slope on actual Earth-space links to LEO should account for the possibility of encountering such steep fade slopes and plan accordingly.

C. Model Validation

Ideally, we would validate our simulation model by comparing its predictions with the results obtained from hundreds

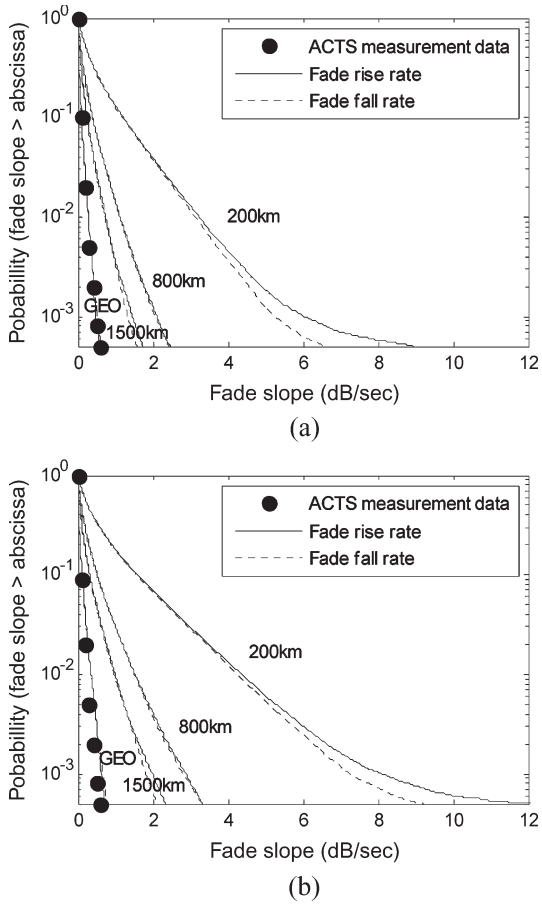

Fig. 7. CCDFs of the fade slope observed on simulated Earth-space links to LEO satellites in 200-, 800-, and 1500-km polar orbits and ACTS in GEO from a site near Tampa, FL. (a) $f = 20$ GHz. (b) $f = 27.5$ GHz.

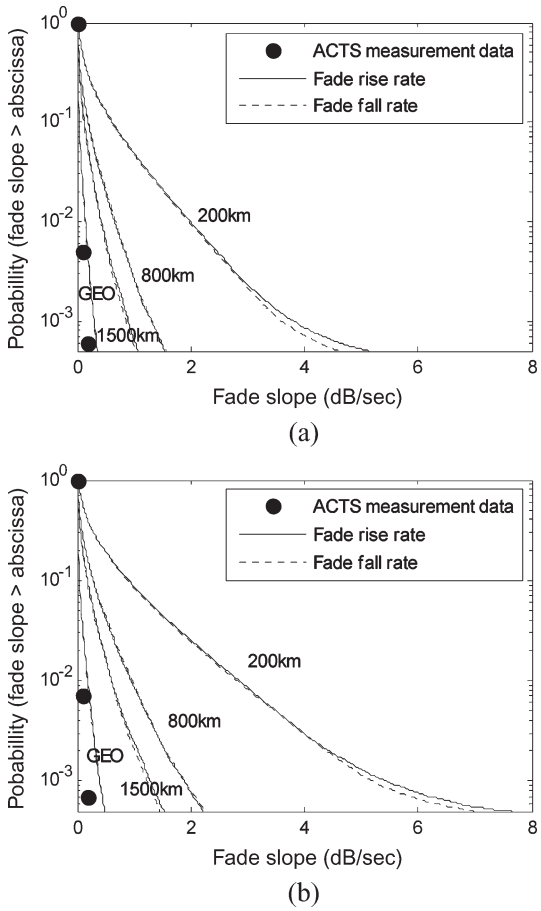

Fig. 8. CCDFs of the fade slope observed on simulated Earth-space links to LEO satellites in 200-, 800-, and 1500-km polar orbits and ACTS in GEO from a site near White Sands, NM. (a) $f = 20$ GHz. (b) $f = 27.5$ GHz.

of hours of measurement data from actual Ka-band Earth-LEO links. Because such data are not yet available, we took a different route and compared our simulator's predictions of the long-term fade slope distributions likely to be observed over geostationary links to Earth stations located at Tampa, FL, and White Sands, NM, with those actually observed at these sites during the Advanced Communications Technology Satellite (ACTS) program [10]. Because the Earth-space path is fixed, we assume that fade slope is solely due to advection of the rain field past the Earth station by the wind. As described in the previous section, we assumed a lognormally distributed wind speed with a median value of 30 km/h and a standard deviation of $\log_e 2$. In a manner similar to our LEO simulations, we ran 3000 simulations, each with a length of 20 min, yielding 1000 h (or 3.6 million s) of time-series data. In processing our data, we used the same ACA threshold as the ACTS team used in processing their data. The results, which are shown in Figs. 7 and 8, are a close match to the measurement data presented in [10]. In the absence of more complete validation data, this gives us confidence that the results of our simulations are likely useful representations of reality.

On Earth-space links to LEO, fade slope is mainly due to the movement of the Earth-space path through the rain field. In Table III, we present estimates of the average speed of the intersection of the Earth-space path with the top of the rain layer as the satellite sweeps across the sky. Because these speeds are so much higher than the median wind speed used in our simulations, it seems reasonable to conclude that simulations of Earth-space links to LEO conducted with a static rain field will essentially yield results that are identical to those obtained with a wind-blown rain field. Our simulation results confirm this. Moreover, this also suggests that the fade slopes encountered by a mobile terminal that moves at conventional speeds (tens of kilometers per hour) and has a clear view of the sky will not be greatly affected by the motion of the terminal and will be comparable to those encountered by fixed or transportable terminals.

D. Fade Slope Analysis

Conditional CCDFs of both rising and falling fade slopes observed on simulated 20- and 27.5-GHz links to satellites in 200-, 800-, and 1500-km polar orbits from Earth stations located near White Sands, NM, and Tampa, FL, are shown in Figs. 7–9. The results suggest that links to LEO will encounter fade slopes that will be twice to ten times greater than those previously reported for links to GEO. In particular, we note that fade slopes become much steeper as 1) the altitude of the satellite decreases (and the angular velocity of the satellite across the sky increases, as suggested in Fig. 10); 2) the

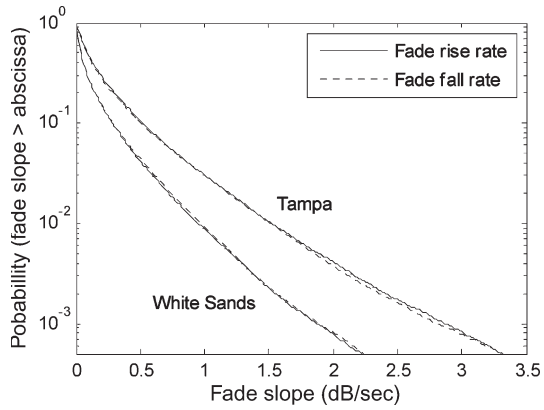

Fig. 9. CCDFs of the fade slope observed on simulated 27.5-GHz Earth-space links to LEO satellites in 800-km polar orbits from sites corresponding to Tampa, FL, and White Sands, NM.

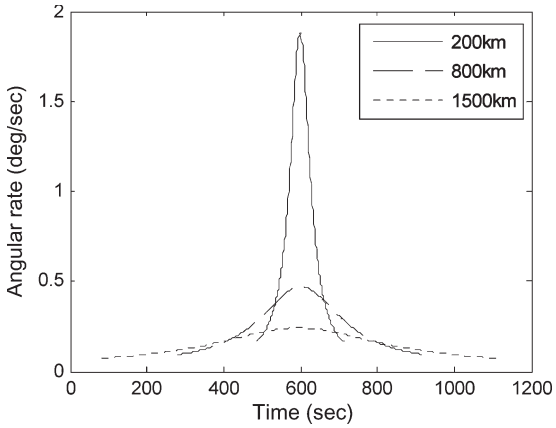

Fig. 10. Apparent angular rates of LEO satellites in 200-, 800-, and 1500-km polar orbits during passes that have a maximum elevation angle of 60°.

carrier frequency increases (the path geometry in our simulation implies that the frequency scaling factor for attenuation will also be the frequency scaling factor for fade slope; this may not be strictly true in practice); and 3) the average rain rate increases (and the rain attenuation increases). Furthermore, our results suggest that rising and falling fade slopes of a given value are equally likely.

Others have found that a lognormal distribution often fits the fade slope distribution on links to GEO, e.g., [9], so we attempted a similar fit here. The result is shown in Fig. 11. In all cases, we found that the lognormal distribution fits well at probability levels > 0.01 but tends to overpredict the probability of observing a given fade slope at probability levels < 0.01. The probability threshold at which the fit is lost increases as the rain rate increases and/or the altitude decreases. The geometry of Earth-LEO links is considerably more complex than that of GEO; detailed analysis of the manner in which the fade slope distribution jointly depends on fade depth, elevation angle, and average rain rate may be a useful topic for further study.

V. Conclusion

We have assessed fade slope statistics on Ka-band Earth-space links using rain field simulations based on Goldhirsh's method for estimating the key parameters of an EXCELL-based model of horizontal rain structure from ITU-R rain rate

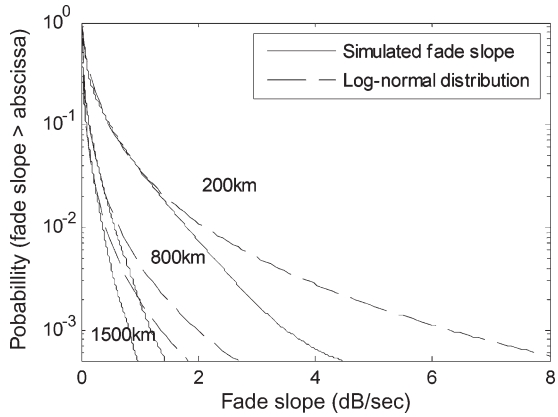

Fig. 11. Best fit of a lognormal distribution to the CCDFs of the fade slope observed on simulated Earth-space links at 20 GHz to LEO satellites in 200-, 800-, and 1500-km polar orbits from a site near White Sands, NM.

statistics and a simple wind velocity model that accounts for advection of the rain cells over time. Despite many simplifying assumptions, our predictions of the fade slope distributions on links to GEO closely match those observed at sites in White Sands, NM, and Tampa, FL, during the ACTS program. This gives us confidence that the fade slope distributions that we have predicted for links to LEO are likely reasonable.

Our results for LEO satellites show that fade slopes will become steeper as 1) the altitude of the satellite decreases; 2) the frequency band of operation increases; and 3) the average rain rate increases. Furthermore, they suggest that, at a given probability level, fade slopes could be between two and ten times greater than those for geostationary satellites. Furthermore, they also suggest that the fade slopes encountered by a mobile terminal that moves at conventional speeds (tens of kilometers per hour) and has a clear view of the sky will see fade slopes that are comparable with those encountered by fixed or transportable terminals.

Although more complex rain field models may ultimately yield more accurate results at specific locations, the predicted fade slope distributions presented here represent a useful starting point for those engaged in the design of fade mitigation techniques, the development of rain field models for use in Earth-space link simulations, or the planning of propagation measurement campaigns involving Ka-band Earth-LEO links. The limitations of our work are largely those of the underlying rain field model. The next logical step is to gradually increase the complexity (and, presumably, the fidelity) of the underlying rain cell model and determine how the fade slope distribution predictions are affected. The ultimate step, of course, would be to obtain statistically significant amounts of measurement data from Ka-band Earth-LEO links to which the predictions presented here could be compared.

Acknowledgment

The authors would like to thank A. R. Razali, for calculating the conditional CCDFs of rain rate for specific locations, and C. Amaya and D. V. Rogers of the Communications Research Centre, Ottawa, ON, Canada, for helpful discussions and comments.

REFERENCES

[1] D. V. Rogers, L. J. Ippolito, Jr., and F. Davarian, "System requirements for Ka-band Earth-satellite propagation data," *Proc. IEEE*, vol. 85, no. 6, pp. 810–820, Jun. 1997.

[2] C. K. Chen and K. Tseng, "ROCSAT-1 Ka-band experimental communication payload operations," in *Proc. AIAA SpaceOps*, Houston, TX, 2002.

[3] T. Kostulski, and S. Reisenfeld, "Ka band propagation experiments on the Australian low-Earth orbit microsatellite 'FedSat,"' in *Proc. 6th Australian Commun. Theory Workshop*, 2005, pp. 102–106.

[4] T. Kostulski, and S. Reisenfeld, "Variable slant-path Ka-band propagation measurements on the Australian LEO microsatellite 'FedSat,"' in *Proc. 11th Ka Broadband Commun. Conf.*, Rome, Italy, Sep. 25–28, 2005, pp. 365–372.

[5] G. Giffin, K. Magnussen, M. Wlodyka, L. Duffield, B. Poller, and J. Bravman, "Cascade: A smallsat system providing global, high quality movement of very large data files," in *Proc. Int. Astronautical Congr.*, Vancouver, BC, Canada, 2004.

[6] P. Lee, K. Magnussen, G. Giffin, M. Wlodyka, D. Michelson, J. Ma, and B. Diallo, "Channel simulation and fade mitigation techniques for LEO Ka-band high speed data links," in *Proc. AIAA Int. Commun. Satellite Syst. Conf.*, San Diego, CA, Jun. 11–14, 2006.

[7] *Statement of Work for the Study of Data Downlink Systems for Earth Observation Satellites Operating in the 26 GHz Band*, ESTEC, Noordwijk, The Netherlands, Mar. 30, 2007. EOP-SFP/2006-03-1260, Issue 1.

[8] F. Rücker, "Frequency and attenuation dependent fade slope statistics," *Electron. Lett.*, vol. 29, no. 9, pp. 744–746, Apr. 1993.

[9] B. Nelson and W. L. Stutzman, "Fade slope on 10 to 30 GHz Earth-space communication links—Measurements and modelling," *Proc. Inst. Elect. Eng.—Microw. Antennas Propag.*, vol. 143, no. 4, pp. 353–357, Aug. 1996.

[10] J. Feil, L. J. Ippolito, Jr., H. Helmken, C. E. Mayer, S. Horan, and R. E. Henning, "Fade slope analysis for Alaska, Florida, and New Mexico ACTS propagation data at 20 and 27.5 GHz," *Proc. IEEE*, vol. 85, no. 6, pp. 925–935, Jun. 1997.

[11] M. M. J. L. van de Kamp, "Statistical analysis of rain fade slope," *IEEE Trans. Antennas Propag.*, vol. 51, no. 8, pp. 1750–1759, Aug. 2003.

[12] A. P. Chambers, S. A. Callaghan, and I. E. Otung, "Analysis of rain fade slope for Ka and V-band satellite links in Southern England," *IEEE Trans. Antennas Propag.*, vol. 54, no. 5, pp. 1380–1387, May 2006.

[13] Iridium Support Center, Iridium Satellite LLC, private communication, Jul. 18, 2007.

[14] C. Capsoni, F. Fedi, C. Magistroni, A. Paraboni, and A. Pawlina, "Data and theory for a new model of the horizontal structure of rain cells for propagation applications," *Radio Sci.*, vol. 22, no. 3, pp. 395–404, May/Jun. 1987.

[15] J. Goldhirsh, "Two-dimension visualization of rain cell structures," *Radio Sci.*, vol. 35, no. 3, pp. 713–729, May/Jun. 2000.

[16] L. Feral, H. Sauvageot, L. Castanet, and J. Lemorton, "HYCELL—A new hybrid model of the rain horizontal distribution for propagation studies—Part I: Modeling of the rain cell," *Radio Sci.*, vol. 38, no. 3, Jun. 13, 2003. 1056, DOI: 10.1029/2002RS002802.

[17] L. Feral, H. Sauvageot, L. Castanet, and J. Lemorton, "HYCELL—A new hybrid model of the rain horizontal distribution for propagation studies—Part 2: Statistical modeling of the rain rate field," *Radio Sci.*, vol. 38, no. 3, Jun. 13, 2003. 1057, DOI: 10.1029/2002RS002803.

[18] L. Feral, H. Sauvageot, L. Castanet, J. Lemorton, F. Cornet, and K. Leconte, "Large-scale modeling of rain fields from a rain cell deterministic model," *Radio Sci.*, vol. 41, no. 2, Apr. 29, 2006. RS2 010, DOI: 10.1029/2005RS003312.

[19] C. Capsoni, L. Luini, A. Paraboni, and C. Riva, "Stratiform and convective rain discrimination deduced from local $P(R)$," *IEEE Trans. Antennas Propag.*, vol. 54, no. 11, pp. 3566–3569, Nov. 2006.

[20] S. Y. Li and C. H. Liu, "An analytical model to predict the probability density function of elevation angles for LEO satellite systems," *IEEE Commun. Lett.*, vol. 6, no. 4, pp. 138–140, Apr. 2002.

[21] *NORAD two-line element sets—Current data*. [Online]. Available: http://celestrak.com/NORAD/elements/

[22] E. Matricciani, "Physical-mathematical model of the dynamics of rain attenuation based on rain rate time series and a two-layer vertical structure of precipitation," *Radio Sci.*, vol. 31, no. 2, pp. 281–295, 1996.

[23] E. Matricciani, "Transformation of rain attenuation statistics from fixed to mobile satellite communication systems," *IEEE Trans. Veh. Technol.*, vol. 44, no. 3, pp. 565–569, Aug. 1995.

[24] E. Matricianni and S. Moretti, "Rain attenuation statistics useful for the design of mobile satellite communication systems," *IEEE Trans. Veh. Technol.*, vol. 47, no. 2, pp. 637–648, May 1998.

[25] E. Matricciani, "Rain attenuation predicted with a two-layer rain model," *Eur. Trans. Telecommun.*, vol. 2, no. 6, pp. 127–715, Nov./Dec. 1991.

[26] M. Thurai and T. Iguchi, "Rain height information from TRMM precipitation radar," *Electron. Lett.*, vol. 36, no. 12, pp. 1059–1061, Jun. 2000.

[27] M. Thurai, E. Deguchi, K. Okamoto, and E. Salonen, "Rain height variability in the tropics," *Proc. Inst. Elect. Eng.—Microw. Antennas Propag.*, vol. 152, no. 1, pp. 17–23, Feb. 2005.

Weiwen Liu received the B.Eng. degree in electrical engineering from Harbin Institute of Technology, Harbin, China, in 2006. She recently completed the M.A.Sc. degree with the Department of Electrical and Computer Engineering, University of British Columbia, Vancouver, BC, Canada.

Her main research interests include propagation and channel modeling for Ka-band satellite communications.

David G. Michelson (S'80–M'89–SM'99) received the B.A.Sc., M.A.Sc., and Ph.D. degrees from the University of British Columbia (UBC), Vancouver, BC, Canada, all in electrical engineering.

From 1996 to 2001, he was a member of a joint AT&T Wireless Services, Redmond, WA, and AT&T Labs—Research, Red Bank, NJ, team that was concerned with the development of propagation and channel models for next-generation and fixed wireless systems. The results of this work formed the basis for the propagation and channel models later adopted by the IEEE 802.16 Working Group on Broadband Fixed Wireless Access Standards. From 2001 to 2002, he helped to oversee the deployment of one of the world's largest campus wireless local area networks at UBC while also serving as an Adjunct Professor with the Department of Electrical and Computer Engineering, UBC. Since 2003, he has led the Radio Science Laboratory, Department of Electrical and Computer Engineering, UBC. His current research interests include propagation and channel modeling for fixed wireless, ultrawideband, and satellite communications.

Dr. Michelson is a Registered Professional Engineer. He serves as the Chair of the IEEE VT-S Technical Committee on Propagation and Channel Modeling and as an Associate Editor for Mobile Channels for the *IEEE Vehicular Technology Magazine*. In 2002, he served as a Guest Editor for two Special Issues of the IEEE JOURNAL ON SELECTED AREAS IN COMMUNICATIONS concerning propagation and channel modeling. From 2001 to 2007, he served as an Associate Editor for the IEEE TRANSACTIONS ON VEHICULAR TECHNOLOGY. From 1999 to 2007, he chaired the IEEE Vancouver Section's Joint Communications Chapter. Under his leadership, the Chapter received the Outstanding Achievement Awards from the IEEE Communications Society in 2002 and 2005 and the Chapter of the Year Award from the IEEE Vehicular Technology Society in 2006. In 2009, he received the E. F. Glass Award from IEEE Canada for his contributions to the IEEE Communications Society and IEEE Vancouver Section.